DESIGN OF A MAGNETICALLY SUSPENDED WHEEL FOR A MINIATURE GYRO MADE USING PLANAR FABRICATION TECHNOLOGIES*

Charles R. Dauwalter
Milli Sensor Systems and Actuators, Inc.
93 Border Street
West Newton, MA 02465-2013

SUMMARY

The technical feasibility of a magnetically suspended rotating wheel for miniature gyro and other applications, which was first investigated under a NASA SBIR contract, was assessed in much greater detail under a BMDO SBIR administered by DTRA. The configuration is amenable to economical and highly reproducible batch fabrication using the rapidly emerging planar fabrication technologies. The actuator for the wheel magnetic suspension was optimized for improved performance by exploring the design space through over 600 configuration variations using a finite difference magnetic circuit analysis technique implemented in a spreadsheet environment. Normal and tangential magnetic force components of circumferentially slotted rotors and stators were determined over a range of air gaps, slot width to tooth width ratios, slot depth to tooth pitch ratios and tangential displacements

INTRODUCTION

The work described herein is an extension of work reported at the 3rd International Symposium on Magnetic Suspension Technology[1]. The principal objective of the new work was to optimize the design of the magnetic actuator for the magnetically suspended wheel, maximize the support force capability, minimize power dissipation and provide approximately equal capability to support accelerations both in the plane of the wheel and perpendicular to it. Secondary objectives were to develop a specific design of variable reluctance drive motor; and determine the maximum feasible rotational speed consistent with allowable stresses in the wheel material.

Our group is pursuing the development of inertial instruments, such as gyros and accelerometers, that can be fabricated through the use of many of the technologies widely used for micro-devices, but adapted for application to larger devices. We have termed these fabrication technologies "millimachining"; they were discussed in the previous paper[2]. Briefly, millimachining is a design philosophy and fabrication approach that MSSA is developing from a merging of the traditional technologies and the emerging micro-machining technology, and applying it to devices in the size range between macro and micro. Millimachined inertial instruments are expected to realize higher performance than micro instruments due to larger angular momentum. Millimachined devices can also be expected to be less expensive and more reliable than conventionally fabricated macro-sized instruments because they can take advantage of the economy and reproducibility of batch processing and dispense with most of the expensive, time consuming and unreliable hands-on human labor.

*The work described was performed under BMDO SBIR Contract DTRA01-96-C-0138

MAGNETICALLY SUSPENDED WHEEL CONFIGURATION

The wheel and actuator configuration that we are pursuing is shown in Figure 1, which shows the wheel assembled with the magnetic suspension actuator quadrants and the "U"-shaped segments of the drive motor stator. This configuration and associated control system are the subject of a recently issued patent[3].

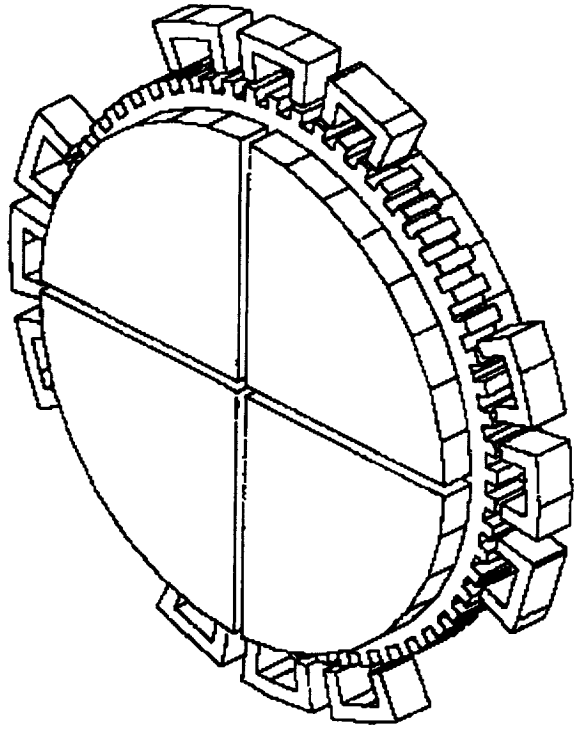

Figure 1. Magnetically suspended wheel and actuator configuration.

Figure 2 shows the assembly with a group of 4 magnetic suspension actuator stators swung away from the wheel. As shown in Figure 2, the wheel has circumferential grooves that enable the generation of forces that are parallel to the actuator/wheel plane, in addition to the forces normal to that plane usually utilized in electromagnetic actuators. The circumference of the wheel has notches, or "teeth" which, in conjunction with the "U"-shaped motor stator segments (the electrical conductors used to excite the cores are not shown in the illustration), constitute a multi-phase variable reluctance motor to drive the wheel in rotation.

Each of the actuator quadrants has matching circumferential grooves which have electrical conductors imbedded in (and electrically insulated from) them. The current in adjacent grooves flows in opposite directions. Passage of electric current through the conductors makes the actuator quadrants electromagnets, which magnetically attract the wheel to the actuator quadrants. Radial forces (parallel to the plane of the actuators) are also produced due to the slight intentional misalignment of the actuator grooves with the wheel grooves. This misalignment can be seen in Figure 3, which is a partial crossection of the wheel and a facing actuator quadrant showing the details of the construction. The grooves in the actuator quadrant are displaced laterally from those of the wheel by approximately 1/2 of the slot pitch, P, (slot pitch is the distance from one edge of a slot to the corresponding edge of the adjacent slot; tooth pitch is similarly defined where the teeth are the projecting portions adjacent to the slots). This is shown more clearly in Figure 4, a crossection view of half of the wheel with its actuators. The misalignment of the teeth (or slots) causes tangential forces (parallel to the air gap; this is in the radial direction of the wheel) as well as normal forces (perpendicular to the air gap) to be generated by the passage of electrical current through the conductors. The tangential forces result from the tendency for the actuator and wheel teeth to become aligned under the influence of the

magnetic field, because the position of minimum magnetic energy, for a given air gap, is when the wheel and actuator teeth are perfectly aligned.

Eight actuator sectors, 4 on each side of the wheel, are provided to generate the forces necessary to support the wheel in 5 degrees of freedom; rotation about the axis of symmetry of the wheel is the sixth degree of freedom. Each actuator sector is capable of generating forces both normal and parallel to the surface facing the wheel.

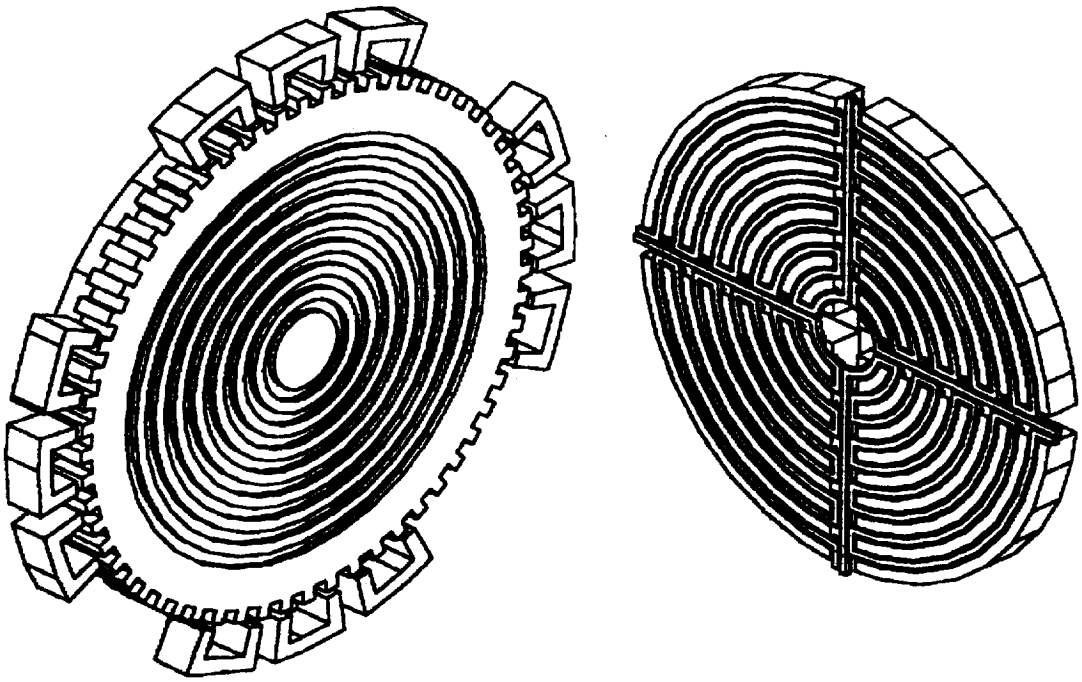

Figure 2. Magnetically suspended wheel and actuator configuration, exploded.

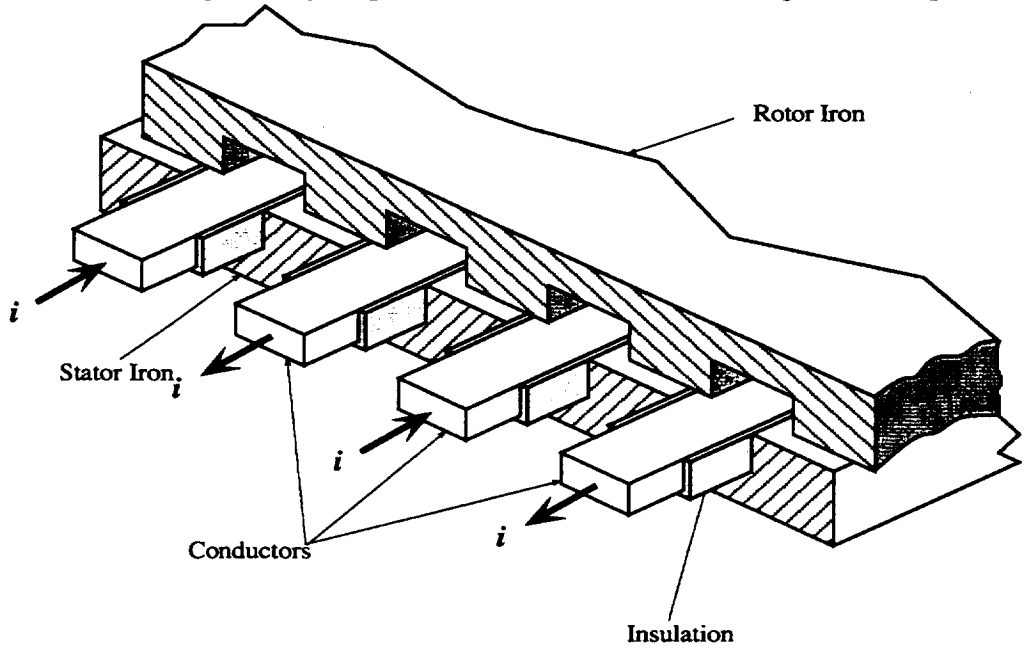

Figure 3. Actuator details.

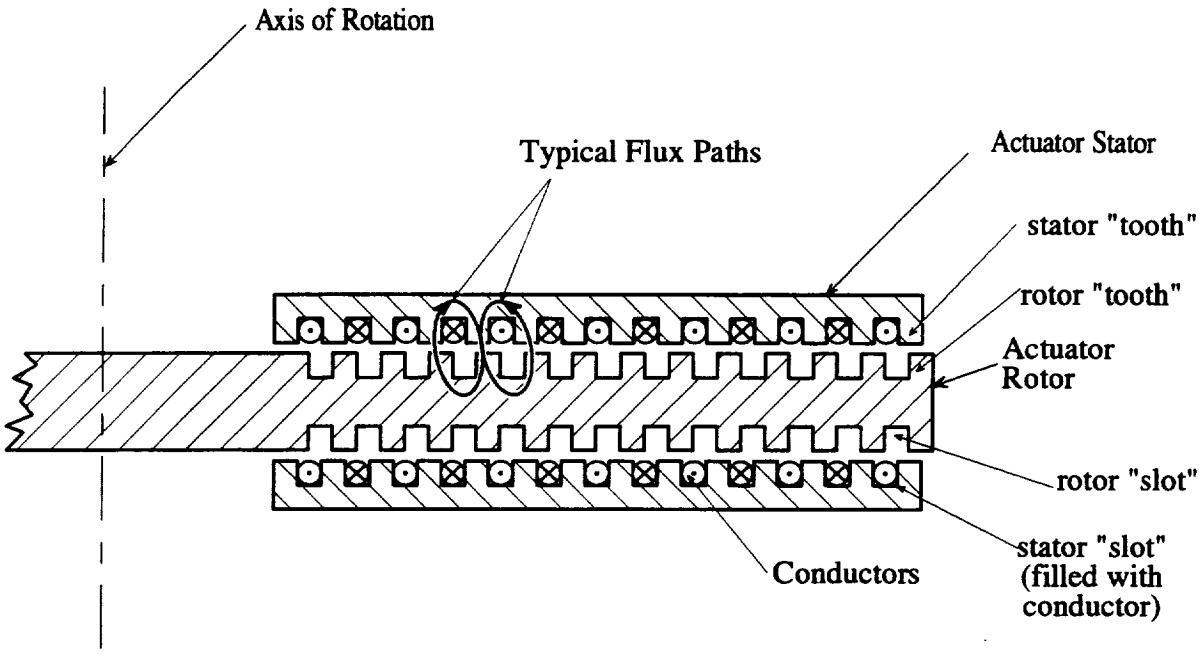

⊗ = current direction into paper

⊙ = current direction out of paper

Figure 4. Wheel and actuator crossection.

PREVIOUS RESULTS

In the previous work, the radial and tangential forces were both found to vary approximately sinusoidally with tangential (parallel to the actuator plane) displacement with a period of the slot pitch, P. The normal and tangential forces are phase shifted by about $\pi/2$, or 1/4 of the slot pitch. Consequently, the normal force is maximum (or minimum) at the tangential displacement at which the tangential force is zero and the tangential force is maximum (or minimum) when the normal force is midway between its extrema. As might be expected, the normal forces were much larger than the tangential forces, resulting in a wheel that had much lower force capabilities (thus linear acceleration capability) in the plane of the wheel than normal to it. In most applications, equal capability in all directions would be necessary, or at least advantageous. With this in mind, the present work was initiated to, among other things, optimize the suspension configuration to achieve, as nearly as possible, equal suspension capabilities in all directions.

PRESENT WORK

Suspension Capability Optimization

The previous work explored the normal and tangential force capability of the actuator configuration in which both the rotor and stator pole widths and slot widths were the same, namely, half of the slot pitch, P. The stator slot depth was 0.25P and the rotor slot depth was 0.375P, and the air gap was varied from

0.09375P to 0.25P. The present work set out to explore the design space more fully in search of a more optimum configuration. To this end, the tooth width to slot width ratio, w_{tooth}/w_{slot}, was varied from 0.1428P to 1.666P, the stator slot width, $w_{slot,stator}$, was varied from 0.25P to 0.75P, the rotor slot width, $w_{slot,rotor}$, was varied from 0.125P to 0.5P, and the air gap, g, was varied from 0.09375P to 0.25P. Over these ranges of parameter values, approximately 600 models were formulated and solved for normal and tangential forces. For most of these models, a slot current value of 1.0 ampere was used, although, as expected, the forces scale as the slot current squared and results from models with other current values could easily be converted to equivalent values at 1.0A.

Results

Force vs. Slot Depths Figure 5 shows the tangential (F_x) and normal (F_y) forces with $w_{tooth}/w_{slot}=1$ as a function of the rotor and stator slot depths at two different tangential displacements. All of this data was generated with $w_{tooth}/w_{slot}=1$. The displacement, x=8, for Figure 5a and Figure 5b are for the rotor displaced P/4 from the condition when the rotor and stator teeth are aligned. This is the displacement where F_x is approximately maximum and F_y is approximately midway between its extrema.

The displacement, x=16, for Figure 5c and Figure 5d are for the rotor displaced P/2 from the condition when the rotor and stator teeth are aligned, that is, for the rotor teeth centered over the stator slots. Here, F_x is essentially zero and F_y has its minimum value (note that in Figure 5c, the force scale has been magnified to show the shape more clearly). In all of these cases, the force dependence on the stator slot depth is negligible. The force dependence on the rotor slot depth is also not very large in any of these cases. For this reason, the stator and rotor slot depths were held at 12/32=0.375 and 8/32=0.25 for exploration of the force dependencies on the w_{tooth}/w_{slot} ratio.

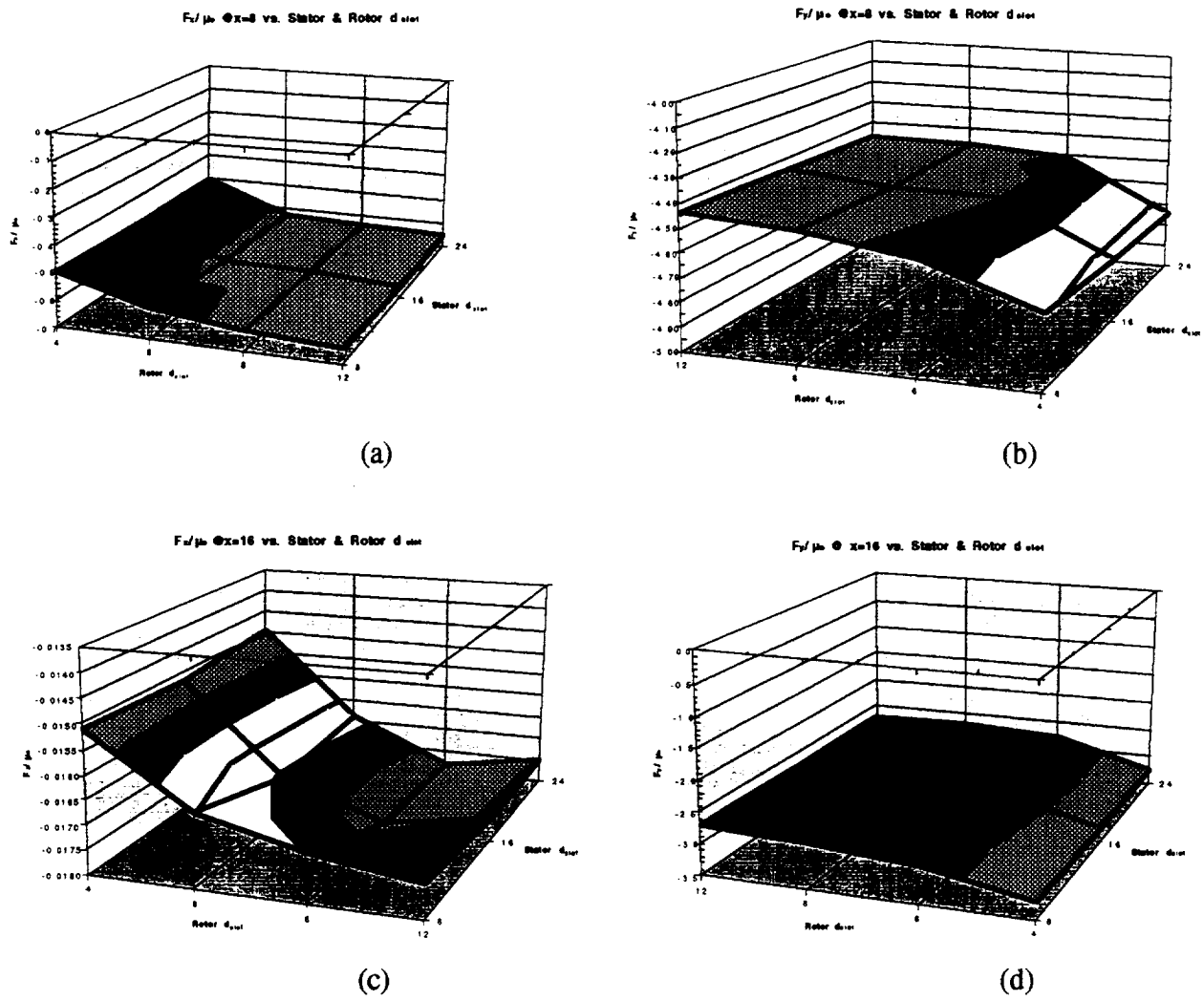

Figure 5. Normal and tangential forces vs. rotor & stator slot depths, 1.0 A slot current.

Force vs. $^{W_{tooth}}/_{W_{slot}}$ *ratio* While the tangential and normal forces vs. air gap were determined for 6 values of the air gap, ranging from 0.09375P to 0.25P, only the results for g=0.125P are presented here because of space limitations. Figure 6 shows the tangential force vs. x at a slot current of 1.0A for the 8 values of $^{W_{tooth}}/_{W_{slot}}$ that were used. While the variation vs. x for all the $^{W_{tooth}}/_{W_{slot}}$ values is roughly sinusoidal, the displacements at which the peak values occur are shifted towards zero, compared to the value at $^{W_{tooth}}/_{W_{slot}}$=1, as the values of $^{W_{tooth}}/_{W_{slot}}$ both increase and decrease from 1. Some of the peak values are larger than for $^{W_{tooth}}/_{W_{slot}}$=1, but only about 20%. Figure 7 shows the normal force vs. x for the same

conditions. Here, all values consistently increase as the slot width is increased and the curves become flatter near the minima as $^{W_{tooth}}/_{W_{slot}}$ becomes both larger and smaller than 1.

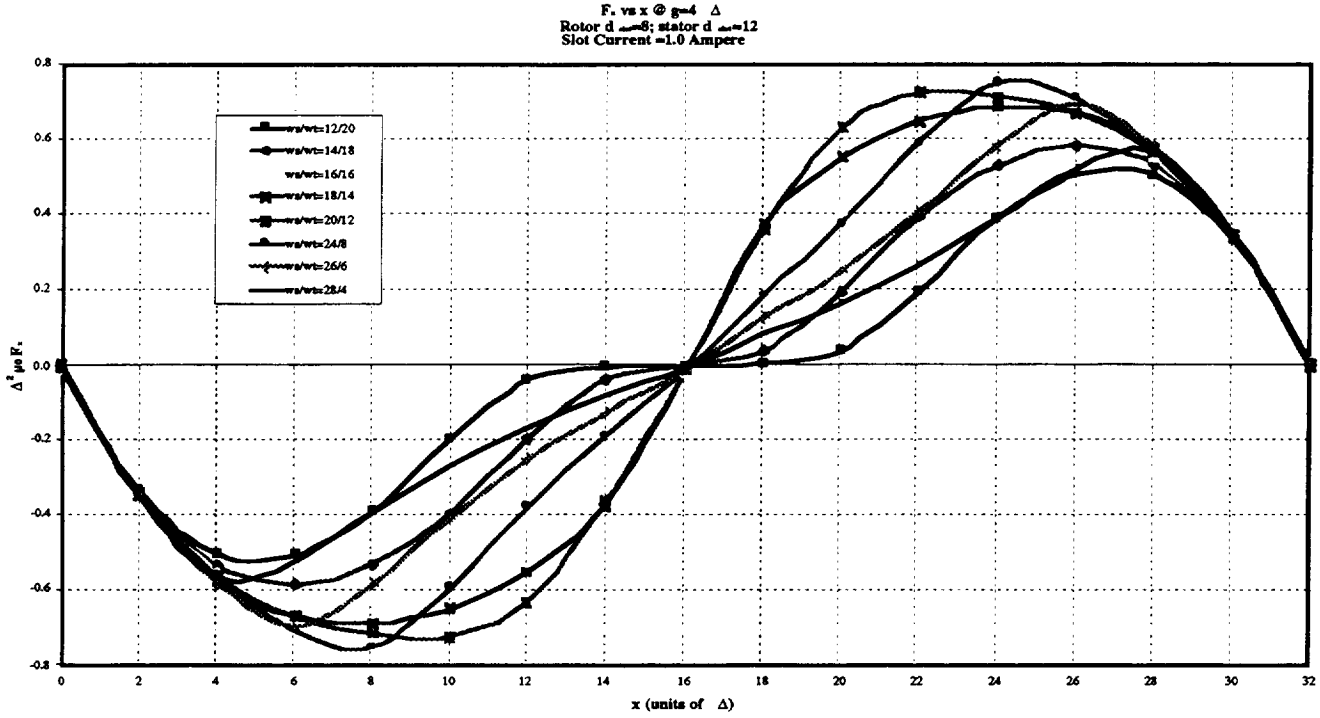

Figure 6. Tangential force vs. x for various $^{W_{tooth}}/_{W_{slot}}$ and I_{slot}=1.0A.

Fx/Fy vs. $^{W_{tooth}}/_{W_{slot}}$ *ratio* Figure 8 shows the ratio of tangential to normal force vs. x. Note that $F_x/(-F_y)$ is plotted to allow easier comparison with the curves for F_x. Recall that the motivation for this work was to increase this ratio so as to make the maximum suspension force capability as nearly equal in the radial and axial directions as practical. Figure 8 shows that the force ratio, $F_x/(-F_y)$, consistently increases as $^{W_{tooth}}/_{W_{slot}}$ is increased. The maximum value, -0.69, occurs near P/4 (tangential displacement of approximately 8 in the graphs) and is 4.95 times larger than the maximum of -0.14 at $^{W_{tooth}}/_{W_{slot}}=1$ as calculated in the earlier work. Achieving such an increase was one of the principal motivations for the work.

Force vs. $^{W_{tooth}}/_{W_{slot}}$ *ratio* Changing the slot width while maintaining the slot current constant, also has the effect of changing the power dissipation, J^2/ρ, since changing the slot area changes J. A useful basis on which to compare various configurations might be the power density on the exposed surface of the device, since both conductive and convective hear transfer depend on the surface area. The temperature rise in the device depends on the heat transfer coefficient as well as the power dissipation. Maintaining the surface power density constant while varying device parameters has the effect of maintaining the device temperature rise constant across the parameter variations. Figure 9 and Figure 10 show the tangential and normal force variations vs. displacement for various $^{W_{tooth}}/_{W_{slot}}$ values, with the surface power density maintained at the same value as for $^{W_{tooth}}/_{W_{slot}}=1$, the value used in the earlier work.

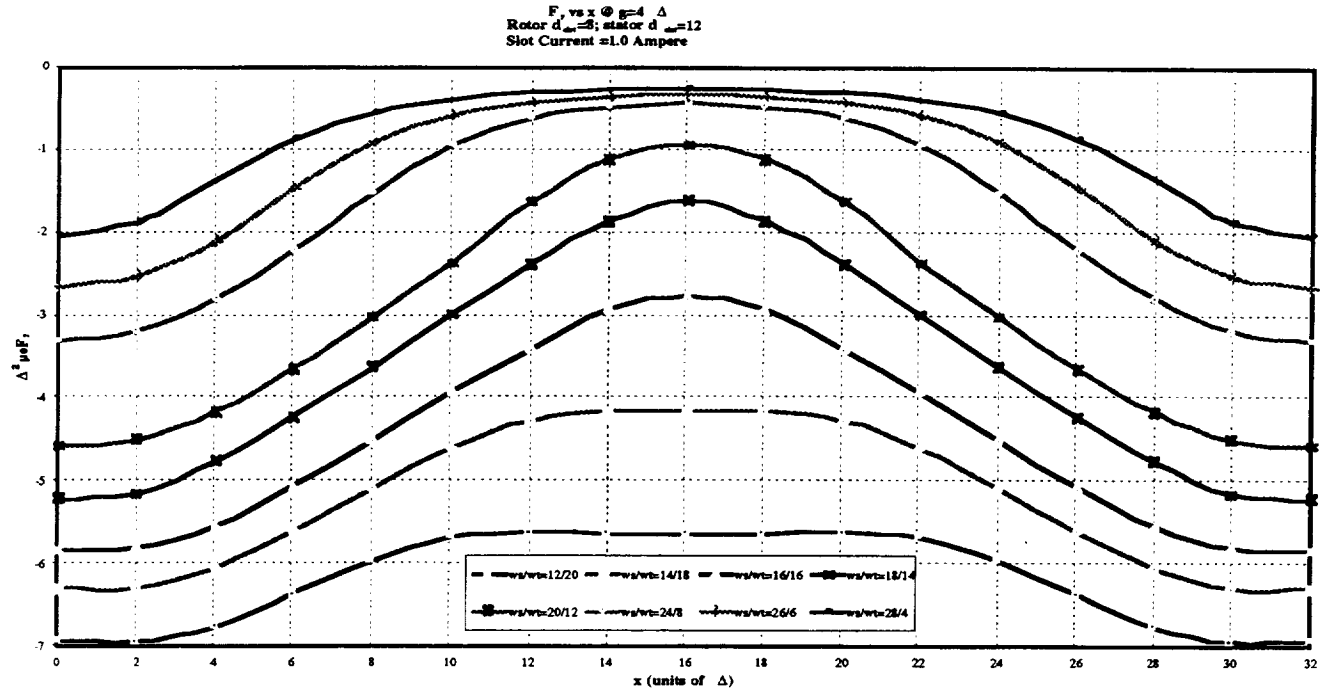

Figure 7. Normal force vs. x for various W_{tooth}/W_{slot} and I_{slot}=1.0A.

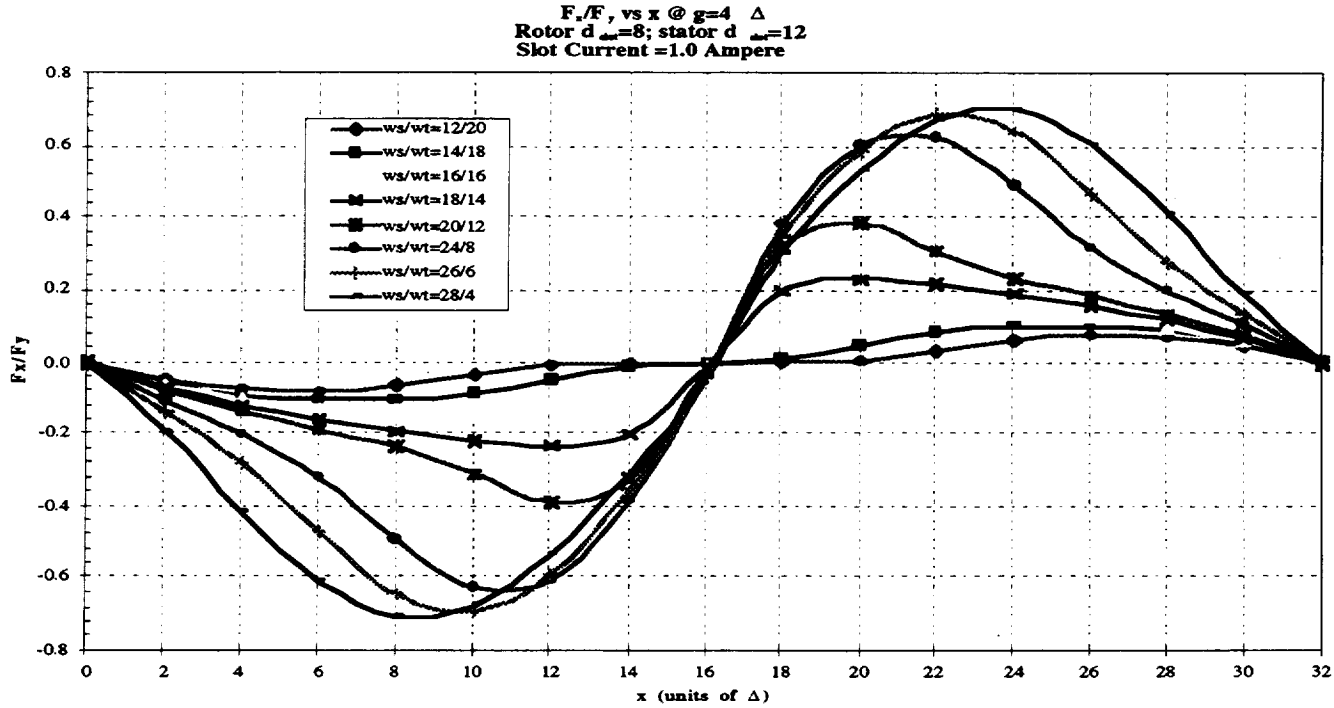

Figure 8. Fx/-Fy vs. x for various W_{tooth}/W_{slot} and I_{slot}=1.0A.

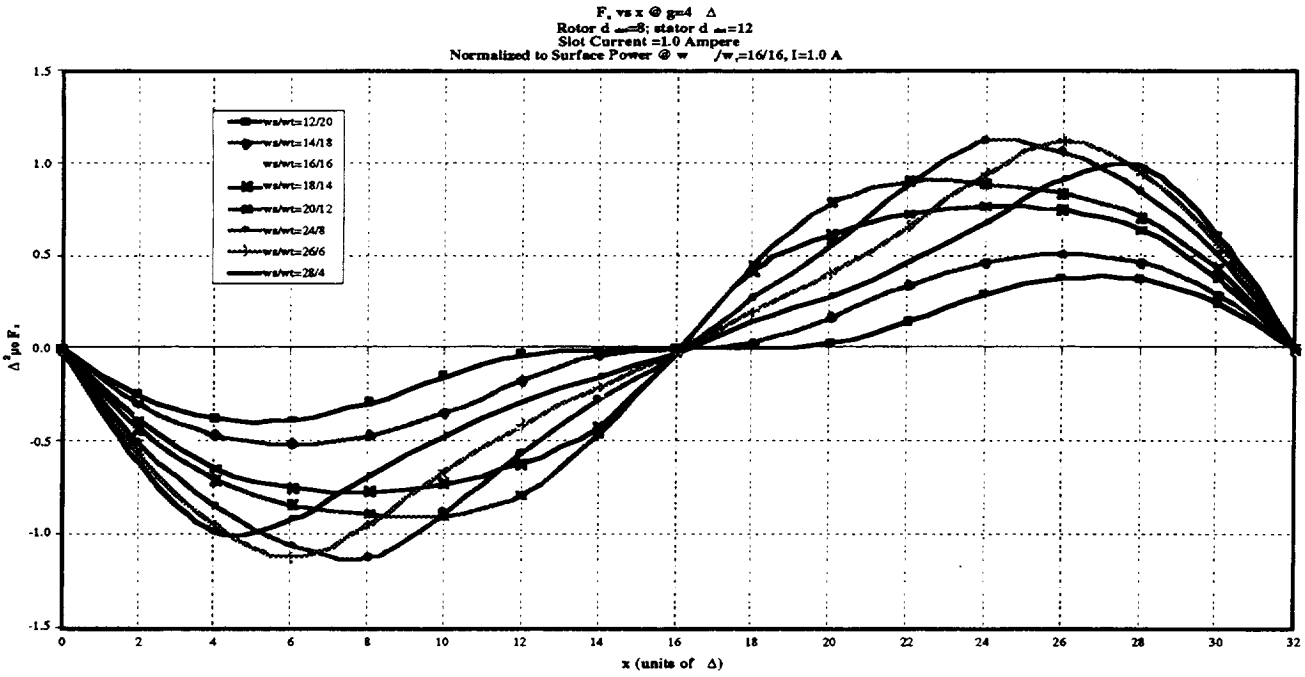

Figure 9. Tangential force vs. x for various W_{tooth}/W_{slot} and I_{slot} normalized to $P_{surface}/A$ = constant.

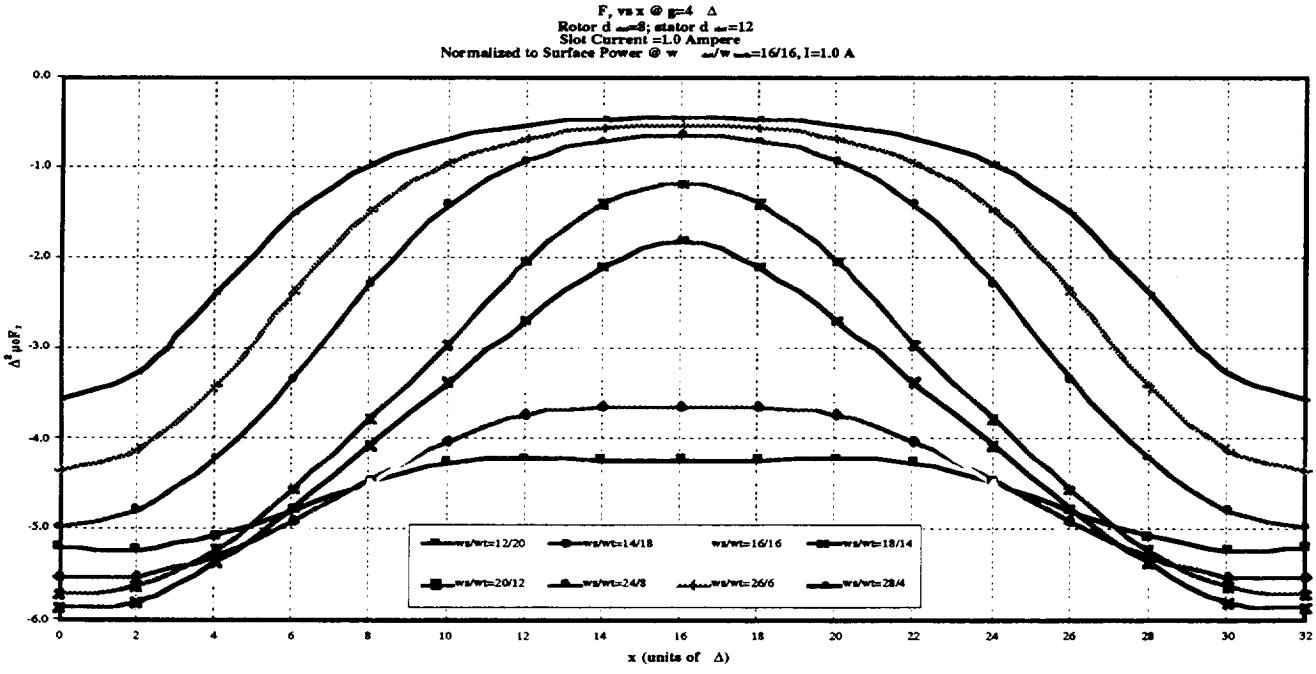

Figure 10. Normal force vs. x for various W_{tooth}/W_{slot} and I_{slot} normalized to $P_{surface}/A$ = constant.

CONCLUSION

The work described thoroughly explored the design space of the magnetic actuator for a magnetically suspended wheel for a miniature gyro and determined the tangential and normal forces for a wide range of design parameter values, including air gap, rotor and stator slot depths and stator and rotor slot widths. The results allow increasing the ratio of tangential to normal force to nearly unity, an improvement of almost a factor of 5 over that of the previous work. This will allow the construction of a magnetically suspended wheel with approximately equal acceleration withstanding capability in all directions, which was one of the principal motivations for the work.

REFERENCES

1. Dauwalter, Charles R., Design of a Magnetically Suspended Wheel for a Miniature Gyro Made Using Planar Fabrication Technologies, Proc. 3rd International Symposium on Magnetic Suspension Technology, Tallahassee, FL, Dec. 1995
2. ibid., pg. 2.
3. U.S. Patent 5,959,382, Magnetic Actuator and Position Control System, Charles R. Dauwalter